

# Gator: a low-background counting facility at the Gran Sasso Underground Laboratory

---

**L. Baudis<sup>a\*</sup>, A.D. Ferella<sup>a</sup>, A. Askin<sup>a</sup>, J. Angle<sup>b</sup>, E. Aprile<sup>c</sup>, T. Bruch<sup>a</sup>, A.Kish<sup>a</sup>, M. Laubenstein<sup>d</sup>, A. Manalaysay<sup>a</sup>, T. Marrodán Undagoitia<sup>a</sup> and M. Schumann<sup>a</sup>**

<sup>a</sup>*Physics Institute,*

*University of Zürich, Winterthurerstrasse 190, CH-8057, Zürich, Switzerland*

<sup>b</sup>*Department of Physics,*

*University of Florida, Gainesville, FL 32611, USA*

<sup>c</sup>*Department of Physics,*

*Columbia University, New York, NY 10027, USA*

<sup>d</sup>*Gran Sasso National Laboratory,*

*Assergi, L'Aquila, 67010, Italy*

*E-mail: laura.baudis@physik.uzh.ch*

**ABSTRACT:** A low-background germanium spectrometer has been installed and is being operated in an ultra-low background shield (the Gator facility) at the Gran Sasso underground laboratory in Italy (LNGS). With an integrated rate of  $\sim 0.16$  events/min in the energy range between 100-2700 keV, the background is comparable to those of the world's most sensitive germanium detectors. After a detailed description of the facility, its background sources as well as the calibration and efficiency measurements are introduced. Two independent analysis methods are described and compared using examples from selected sample measurements. The Gator facility is used to screen materials for XENON, GERDA, and in the context of next-generation astroparticle physics facilities such as DARWIN.

**KEYWORDS:** HPGe spectrometers; low level  $\gamma$ -ray spectrometry.

---

\*Corresponding author.

---

## Contents

<b>1. Introduction</b>	<b>1</b>
<b>2. The Gator facility</b>	<b>2</b>
<b>3. Calibration measurements and efficiency determination</b>	<b>5</b>
<b>4. Data analysis methods</b>	<b>6</b>
4.1 Analysis of gamma-lines	7
4.2 Fit of the data to a simulated spectrum	8
<b>5. Results</b>	<b>9</b>
5.1 Background Analysis	9
5.2 Sample Analysis	10
<b>6. Summary</b>	<b>12</b>
<b>7. Acknowledgements</b>	<b>14</b>

---

## 1. Introduction

Gamma-ray spectroscopy offers a standard method for material screening and selection for rare-event searches, such as the direct detection of Weakly Interacting Massive Particles (WIMPs) [1] or the search for the neutrinoless double beta decay [2]. An ultra-low level germanium spectrometer in a dedicated low-background shield (the Gator facility) has been built and installed at the Laboratori Nazionali del Gran Sasso (LNGS), Italy. While the facility is being operated mainly in the context of the XENON program [3][4][5] [6], recently it also has been used for the GERDA experiment [7] as well as for R&D purposes within low-background particle astrophysics.

This paper is organized as follows: in the next section, the Gator facility is described in detail. In the third section, calibration measurements, efficiency determinations for the different sample geometries, and cross-checks with standard, calibrated samples are described. In the fourth section, two different data analysis methods are introduced. The fifth section describes the determination of the main background sources of the facility as well as selected results for sample measurements. In the final section, a summary and discussion of future plans are presented.

## 2. The Gator facility

The design of the facility has been inspired by the layout of the world's most sensitive germanium spectrometers, operated at LNGS in connection with the Borexino and GERDA experiments [8][9]. The core consists of a high-purity, p-type coaxial germanium (HPGe) detector with 2.2 kg of sensitive mass with a relative efficiency of 100.5%<sup>1</sup>. The detector construction has been performed in close cooperation with Canberra semiconductors [11], using only materials with ultra-low intrinsic radioactive contamination. The cryostat is made of ultra-low activity, oxygen-free copper with the cooling provided by a copper dipstick ('cold finger') in thermal contact with a liquid nitrogen bath. The cryostat is of U-type, with the cooling rod shaped in a right angle below the cryostat to avoid direct line-of-sight to the outside (see Figure 1). While the field-effect transistor (FET) used for the charge readout is cooled and close to the detector, the preamplifier is placed outside the low-background shield, since it contains more radioactive components.

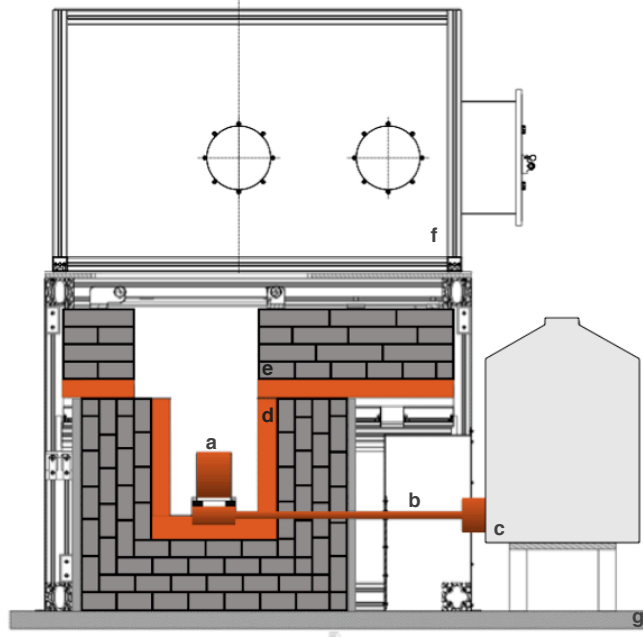
The shield of the detector has been designed to provide a large sample capacity, an ultra-low background and easy access to the germanium spectrometer itself. The sample chamber, with a dimension of  $25 \times 25 \times 33 \text{ cm}^3$ , is surrounded by 5 cm (7 cm for the base plate) of oxygen-free, radio-pure copper from Norddeutsche Affinerie [12]. Residual surface contaminations of the copper plates were removed by treating them with diluted sulfuric and citric acid solutions, followed by cleaning with deionized water. All steps were performed under clean-room conditions. The copper is surrounded by four layers of lead from Plombum [13], each 5 cm thick. The inner 5 cm lead layer has a nominal  $^{210}\text{Pb}$  activity of 3 Bq/kg, while the outer 3 layers were built from lead with a higher  $^{210}\text{Pb}$  activity of 75 Bq/kg. All lead bricks were cleaned with ethanol before being installed in the shield. Their arrangement is such that no direct line-of-sight to the HPGe detector is possible. Large copper plates, which close the sample cavity and carry the upper lead bricks, were placed on sliding rails allowing for easy opening and closing of the shield: The full sample chamber can be accessed when the top shield is open. The lead is surrounded by 5 cm of polyethylene as a shield against ambient neutrons, and the entire shield is enclosed in an airtight aluminum box in order to prevent radon entering the system.

Figure 1 shows a schematic view of the detector and shield configuration. A sample handling and glove box made of plexiglass, including an airlock system, is placed on top of the aluminum housing. The entire system is continuously flushed at slight over-pressure with boil-off nitrogen gas to suppress radon diffusion into the shield. A 5 mm inner diameter PTFE tube allows sealed calibration sources to be brought close to the germanium detector. The samples to be screened are first cleaned in an ultra-sonic bath of ethanol (where applicable), then enclosed in a sealed plastic bag for transportation to the underground site, after which they are stored for a few days under nitrogen atmosphere above the closed chamber. This allows trapped radon and plate-out  $^{220}\text{Rn}$  and  $^{222}\text{Rn}$  progenies to decay before the actual counting starts.

To remotely check the stability of the detector with time, a monitor system has been installed. The liquid nitrogen level, the flow of nitrogen gas, the leakage current across the germanium diode and the high-voltage applied to the diode are read every 2 minutes, while the overall trigger rate is read every 6 hours. The liquid nitrogen level is measured with a level-meter consisting of two 40 cm

---

<sup>1</sup>The quoted efficiency is defined relative to a  $7.62 \text{ cm} \times 7.62 \text{ cm}$  NaI(Tl) crystal, for the 1.33 MeV  $^{60}\text{Co}$  photo-peak, at a source-detector distance of 25 cm [10].



**Figure 1.** Schematic figure of the Gator facility at LNGS. The HPGe detector (a) with its cold finger (b) and dewar (c), the open sample chamber, the copper (d) and lead (e) shield with the sliding door, the glove box (f) and polyethylene shield (g) can be seen.

long concentric metal tubes acting as a capacitor whose capacitance is read out with a universal transducer interface board. The nitrogen gas flow into the shield is monitored and regulated with an electronic flowmeter and the leakage current is measured as the voltage drop across the feedback resistor and read out with an analog-to-digital converter. The relevant parameters are plotted versus time and can be monitored on a web interface which is refreshed every 10 minutes. In case pre-defined thresholds for these parameters are not met, email and SMS alarms are being issued. The data acquisition consists of a high-voltage unit, a spectroscopy amplifier, and a self triggering, 16 k channel multichannel analyzer. The spectra, acquired and cleared every 6 hours, are saved in ascii files and analyzed offline.

Prior to its installation at LNGS, the germanium spectrometer was operated in the Soudan underground laboratory in northern Minnesota, within the SOLO facility [14]. At the Soudan laboratory, the detector was used for the screening of XENON10 [3] materials, and several background runs were acquired [15]. During its water- and ground-based transportation to LNGS, the detector was exposed for several months to the cosmic ray flux at the Earth's surface, leading to cosmic activation of the crystal and the surrounding copper of the cryostat. The shield was improved in October 2008, and it was cleaned once again in February 2009.

Table 1 shows the integral background in the 100-2700 keV region in the Soudan configuration, and for three measurements taken at LNGS. The integral counting rate at LNGS has been constantly decreasing due the decay of cosmogenic radio-nuclides such as  $^{54}\text{Mn}$ ,  $^{57}\text{Co}$ ,  $^{58}\text{Co}$  and  $^{65}\text{Zn}$ , with typical half-lives around one year on the one hand, and due to an improved shield and overall

sealing of the system on the other hand. This is reflected in the decrease of prominent lines from  $^{214}\text{Bi}$  and  $^{214}\text{Pb}$ , as shown in Table 2. It gives the integral counting rates in the  $\pm 3\sigma$ -regions for the main primordial  $\gamma$ -lines, as well as for the  $^{137}\text{Cs}$ ,  $^{60}\text{Co}$  and  $^{40}\text{K}$  lines, along with a comparison with the GeMPI detector, which is one of the world's most sensitive low-background spectrometers [8].

**Table 1.** Integral background counting rates for Gator as measured at Soudan and at LNGS in three different runs. The integral is evaluated in the energy range [100, 2700] keV.

Run	Lifetime [days]	Rate [events/min]
Gator at Soudan	22.96	$0.842 \pm 0.005$
Gator at LNGS (09-2007)	14.90	$0.258 \pm 0.003$
Gator at LNGS (10-2008)	22.59	$0.186 \pm 0.003$
Gator at LNGS (04-2010)	51.43	$0.157 \pm 0.001$

**Table 2.** Background counting rates (in events/day) in the  $\pm 3\sigma$ -regions for the main primordial and the gamma lines of  $^{137}\text{Cs}$ ,  $^{60}\text{Co}$  and  $^{40}\text{K}$ .

Energy [keV]	Chain/nuclide	Peak integral background rate [counts/day]				GeMPI [8]
		Gator (Soudan)	Gator (LNGS, 09-2007)	Gator (LNGS, 10-2008)	Gator (LNGS, 04-2010)	
239	$^{232}\text{Th}/^{212}\text{Pb}$	$1.1 \pm 0.7$	$0.7 \pm 0.1$	$0.13 \pm 0.08$	$<0.5$	NA
911	$^{232}\text{Th}/^{228}\text{Ac}$	$0.9 \pm 0.3$	$0.4 \pm 0.2$	$0.4 \pm 0.1$	$<0.5$	$<0.2$
352	$^{238}\text{U}/^{214}\text{Pb}$	$4.9 \pm 0.7$	$4.3 \pm 0.7$	$1.1 \pm 0.2$	$0.7 \pm 0.3$	$<0.5$
609	$^{238}\text{U}/^{214}\text{Bi}$	$4.5 \pm 0.5$	$4.0 \pm 0.5$	$1.1 \pm 0.2$	$0.6 \pm 0.2$	$0.50 \pm 0.45$
1120	$^{238}\text{U}/^{214}\text{Bi}$	$1.6 \pm 0.3$	$2.7 \pm 0.4$	$1.3 \pm 0.2$	$0.3 \pm 0.1$	NA
1765	$^{238}\text{U}/^{214}\text{Bi}$	$1.3 \pm 0.2$	$1.5 \pm 0.3$	$0.2 \pm 0.1$	$0.08 \pm 0.06$	NA
662	$^{137}\text{Cs}$	$2.9 \pm 0.4$	$0.5 \pm 0.3$	$<0.5$	$0.3 \pm 0.1$	NA
1173	$^{60}\text{Co}$	$0.5 \pm 0.1$	$0.5 \pm 0.2$	$0.5 \pm 0.2$	$0.5 \pm 0.1$	$0.6 \pm 0.4$
1332	$^{60}\text{Co}$	$0.6 \pm 0.1$	$0.6 \pm 0.2$	$0.5 \pm 0.1$	$0.5 \pm 0.1$	$0.4 \pm 0.3$
1461	$^{40}\text{K}$	$5.8 \pm 0.4$	$0.5 \pm 0.2$	$0.4 \pm 0.1$	$0.5 \pm 0.1$	$0.6 \pm 0.4$
2615	$^{208}\text{Tl}$	$0.7 \pm 0.1$	$0.2 \pm 0.1$	$0.2 \pm 0.1$	$0.2 \pm 0.1$	NA

Figure 2 (top) shows the comparison between the latest background spectrum acquired at LNGS (2010), a spectrum taken in the SOLO facility at Soudan (2007) and the background of the GeMPI detector [8]. It also shows (bottom) the Gator spectrum underground at LNGS prior to its installation in the shield, inside the shield, and inside the shield with the radon protection system on. The background decrease is more than four orders of magnitude, and shows that a careful shielding is needed even when the detector is operated deep underground.

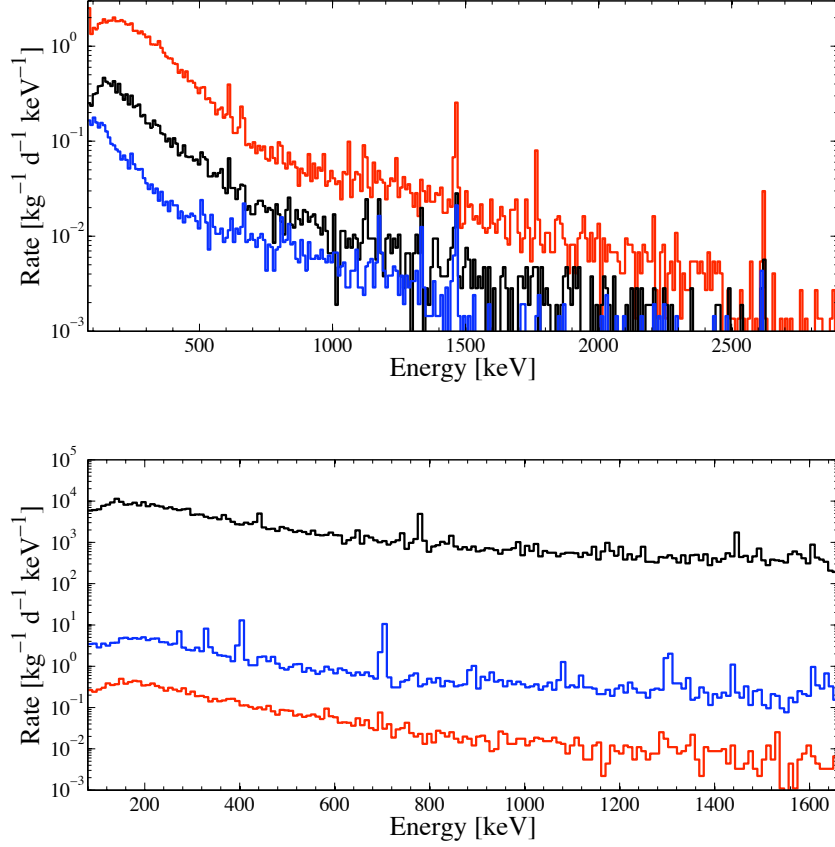


**Figure 2.** (Top) Background spectra of Gator at Soudan (red), at LNGS (black) and the spectrum of the GeMPI detector [8] (blue). (Bottom) Gator background spectrum at LNGS: outside the shield (black), inside the shield (blue) and inside the shield with the radon protection system on (red), clearly showing the suppression of the main gamma lines associated with radon decays.

### 3. Calibration measurements and efficiency determination

The HPGe detector is calibrated regularly with radioactive sources such as  $^{109}\text{Cd}$ ,  $^{133}\text{Ba}$ ,  $^{137}\text{Cs}$ ,  $^{60}\text{Co}$ ,  $^{57}\text{Co}$ ,  $^{22}\text{Na}$ ,  $^{54}\text{Mn}$  and  $^{228}\text{Th}$ . In Figure 3 (left) the comparison of the spectrum obtained from a  $^{60}\text{Co}$  calibration with the one from a Monte Carlo simulation of the source-detector geometry is shown. The FWHM of the two  $^{60}\text{Co}$  lines at 1173 keV and 1332 keV are 2.5 keV and 3.0 keV, respectively. The energy resolution of the detector, defined here as the ratio of the  $\sigma$  to the mean energy of the gamma line, is shown in Figure 3 (right).

The calculation of the detection efficiencies of the various gamma lines used in the analysis of the experimental data (see Section 4) is based on Monte Carlo simulations using Geant4 [16]. For each measured sample, a detailed geometry is included into a Geant4 model of the facility. The efficiency  $\varepsilon$  of a specific  $\gamma$ -line is defined as the ratio between the number of events detected in the line to the number of gammas of that energy emitted by the source. In order to simulate each decay chain, the G4RadioactiveDecay class, which takes into account the branching ratios for the different gamma lines in one decay, is used.

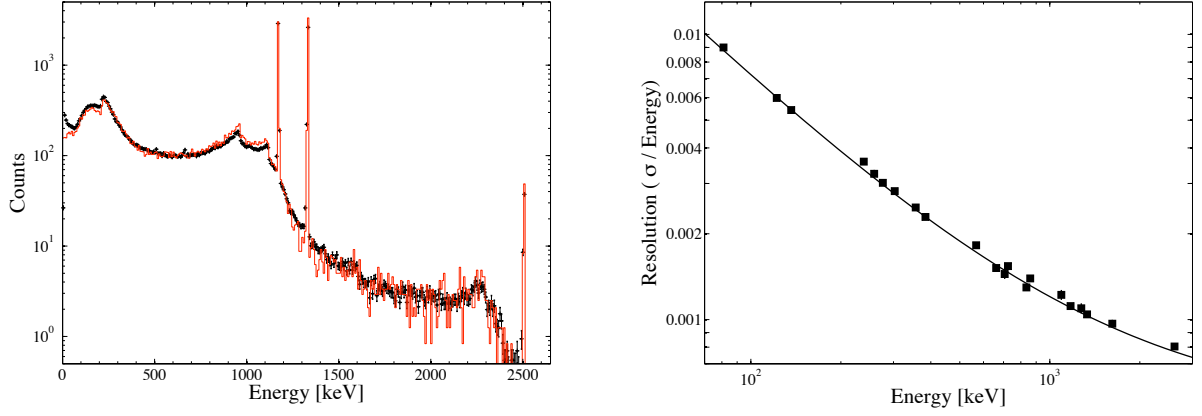


**Figure 3.** (Left) Comparison of the Gator spectrum from a  $^{60}\text{Co}$  calibration (black, data points) with the one from a Monte Carlo simulation of the source-detector geometry (red, solid). (Right) Energy resolution (defined here as the ratio of  $\sigma/\text{energy}$ ) as a function of energy. The solid curves represent a fit using the function  $\sigma^2(E) = E^2(2.35 \times 10^{-7}) + E(7.70 \times 10^{-4}) + (4.43 \times 10^{-1})$ .

To cross-check the efficiency determination, a measurement of two extended sources and a comparison with the certified values for their activities has been performed. The sources used for this measurements, which had similar dimensions and weights, are CANMET-STSD2 (from the Canada Centre for Mineral and Energy Technology) and IAEA-Soil6 (from the International Atomic Energy Agency). Both sources are soils from different places on Earth, which have been thermally treated and sieved several times in order to destroy any remaining organic matter. The homogeneity of the material is certified by the provider. Tables 3 shows the results Gator's screening of these two sources and a comparison with the certified values. Within the uncertainties of the measurements, we find a good agreement. We also show in Figure 3 the comparison of the efficiencies as determined by the Monte Carlo method, with those from the data, as a function of energy, as well as the relative difference among these.

These results indicate that the measurements performed with our spectrometer provide a reliable value for the activity of a given sample. Further cross-check were done by using well-calibrated, commercially available point sources.

#### 4. Data analysis methods

Two methods are used to determine the concentrations of radioactive nuclides in a given sample. In the first method, the most prominent  $\gamma$ -lines are analyzed, using efficiencies as determined by a full Monte Carlo simulation. In the case of  $^{238}\text{U}$ , the  $\gamma$ -lines from the daughters of  $^{226}\text{Ra}$  ( $^{214}\text{Pb}$  and  $^{214}\text{Bi}$ ) and in case of  $^{232}\text{Th}$  the  $\gamma$ -lines from  $^{228}\text{Ac}$  and from  $^{212}\text{Pb}$ ,  $^{212}\text{Bi}$  and  $^{208}\text{Tl}$  are used. In the second method, the overall data spectrum is compared to the one obtained from a Monte Carlo simulation, after subtracting the measured background spectrum, and the activities are determined from the best fit. The results from the two methods agree within the statistical errors, as shown in Section 5. Both methods are explained in more detail below.

**Table 3.** Results from screening the CANMET-STSD2 (493 g) and IAEA Soil6 (530 g) sources and comparison with certified values provided by two agencies (for details, see text).

Nuclide	STSD2 Activity [Bq/kg]	
	Gator results	Certified values
$^{228}\text{Th}$	$75 \pm 4$	$70 \pm 5$
$^{226}\text{Ra}$	$230 \pm 30$	$230 \pm 10$
$^{40}\text{K}$	$590 \pm 10$	$540 \pm 20$
Nuclide	Soil6 Activity [Bq/kg]	
	Gator results	Certified values
$^{226}\text{Ra}$	$88 \pm 5$	$80 \pm 7$
$^{137}\text{Cs}$	$57 \pm 2$	$54 \pm 2$

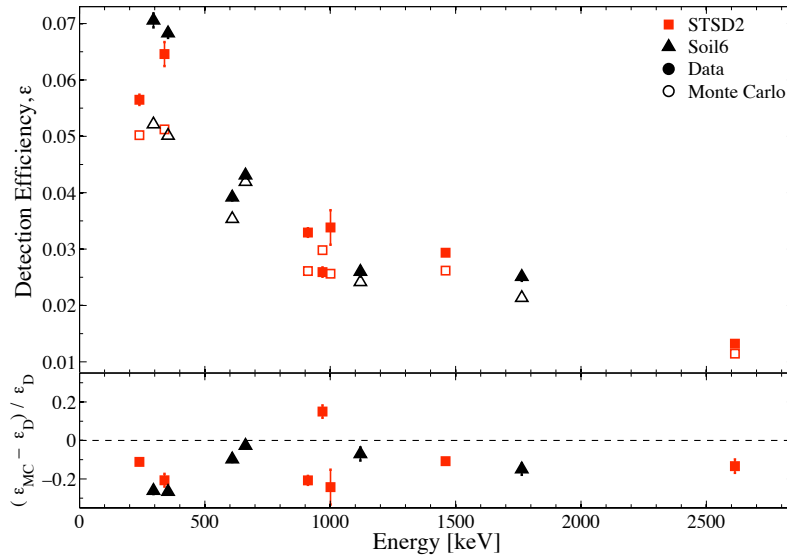


**Figure 4.** Upper panel: Efficiencies as a function of energy for the two certified sources, as determined from data (filled symbols) and Monte Carlo (open symbols). Lower panel: relative difference between simulated (MC) and measured (D) efficiencies.

#### 4.1 Analysis of gamma-lines

The first method is based on counting events at the location of the most prominent lines, after subtracting the background spectrum closest in time. The Compton background, estimated from the regions left and right of a peak, is subtracted as well. The decision on whether the signal exceeds the background is based on comparing the net signal number of counts

$$S_{net} = S - B \cdot t_S / t_B - B_C \quad (4.1)$$

with the so-called detection limit  $L_d$  (the level of a true net signal that can be detected with a given



probability) as defined in [18] for a  $\sim 95\%$  C.L.:

$$L_d = 2.86 + 4.78 \sqrt{B_C + B \cdot \frac{t_S}{t_B} + 1.36}. \quad (4.2)$$

$S$  is the number of counts in the  $\pm 3\sigma$ -region around a peak,  $B$  and  $B_C$  are the number of background and Compton-background counts in the same region, and  $t_S$ ,  $t_B$  are the measuring times for signal and background, respectively. For each peak, three cases are considered [18]:

1.  $S_{net} < 0$ : the upper limit is set to  $L_d$  (no net contribution from a signal)
2.  $0 < S_{net} < L_d$ : the upper limit is set to  $S_{net} + L_d$  (there is an indication of a signal, but it can not be confirmed for the existing background level and sample exposure)
3.  $S_{net} > L_d$ : the detection limit is exceeded (clear indication for a signal at 95% C.L.)

For the third case, the specific activity and its 1  $\sigma$  error is calculated as

$$A[\text{Bq/kg}] = \frac{S_{net}}{r \cdot \varepsilon \cdot m \cdot t} \quad \text{with} \quad \frac{\Delta A}{A} = \frac{\Delta S_{net}}{S_{net}}. \quad (4.3)$$

with the peak efficiencies  $\varepsilon$  as determined by Monte Carlo simulations, the branching ratio  $r$  for the specific line, the mass  $m$  of the sample (in kg), and the measuring time  $t$  (in seconds). For the case in which an upper limit is reported,  $S_{net}$  is replaced by  $L_d$  or by  $(S_{net} + L_d)$  in equation (4.3). As concrete examples, we show the above quantities in Table 4, together with the determined specific activities or upper limits for a copper and a stainless steel sample, using different gamma lines from their measured spectrum.

**Table 4.** Examples of upper limit or specific activities calculation. Details are given in the text.

Sample	Used line [keV]	$S_{net}$	$B \cdot t_S/t_B$	$B_C$	$L_d$	Condition	Activity [mBq/kg]
Copper	239	0	0	93	49	$S_{net} < L_d$	$< 0.33$
	352	-5	19	71	48	$S_{net} < L_d$	$< 0.36$
	1173	42	6	19	27	$S_{net} > L_d$	$0.24 \pm 0.06$
Stainless steel	352	66	7	58	42	$S_{net} > L_d$	$4.3 \pm 0.9$
	1173	236	2	19	25	$S_{net} > L_d$	$7.2 \pm 0.9$
	1461	-3	3	10	21	$S_{net} < L_d$	$< 5.7$

## 4.2 Fit of the data to a simulated spectrum

The individual activities are also determined by a global fit based on a  $\chi^2$ -minimization of the simulated spectrum to the experimental data. The aim is to model  $\vec{y}$ , the measured number of counts in each energy bin, as a function of  $\vec{x}$ , the energy bin value from the Monte Carlo simulation, with a functional dependence of the form

$$\vec{y} = \sum_{k=0}^M a_k \cdot f_k(\vec{x}), \quad (4.4)$$

where  $M$  is the number of simulated radioactive isotopes.  $a_k \geq 0$  are the scaling factors for each isotope, which are kept as free parameters, and  $f_k(\vec{x})$  are  $M$  Monte Carlo spectra which are already smeared with the energy resolution of the detector. For uncorrelated statistical errors in each energy bin  $i$ , the  $\chi^2$  value is defined as

$$\chi^2 = \sum_{i=0}^N \frac{[y_i - \sum_{k=0}^M a_k \cdot f_k(x_i)]^2}{\sigma_i^2}, \quad (4.5)$$

where  $\sigma_i = \sqrt{y_i}$  is the variance in the observed number of counts in each bin and  $N$  is the number of energy bins over which the fit is performed. The statistical uncertainty in the Monte Carlo component is negligible. Before the analysis, the measured background spectrum is subtracted from the sample spectrum. The outcome of this procedure are the scaling factors  $a_k \pm \Delta a_k$  for every decay chain/isotope  $k$ . In the subsequent analysis, these factors are assumed to describe a normalized Gaussian probability distribution function (PDF) with mean  $a_0 = a_k$  and  $\sigma = \Delta a_k$ .

The method applied to decide between a real detection and an upper limit is based on [17]. If the lower of the two symmetric limits providing 95% statistical coverage is positive, a peak detection is claimed and the activity is calculated from  $a_k$ , taking into account the measuring time  $t$  in seconds, the sample mass  $m$  in kg, and the number of simulated events  $n_{sim}$ . The relative  $\pm 1\sigma$  error is given by  $\Delta a_k / a_k$ :

$$A_k [\text{Bq/kg}] = \frac{n_{sim} a_k}{m t} \quad \text{with} \quad \frac{\Delta A_k}{A_k} = \frac{\Delta a_k}{a_k}. \quad (4.6)$$

If the lower limit is equal or less than zero, no detection can be claimed at 95% C.L. and an upper limit is given. Its value  $a_{up}$  is determined by the 95% quantile of the positive part of the Gaussian PDF defined by  $a_0 = a_k$  and  $\sigma = \Delta a_k$ . The limit on the activity (95% C.L.) is calculated using  $a_{up}$  in equation (4.6).

As an example, Figure 4.2 shows a measurement of a stainless steel sample: the data spectrum is compared with the Monte Carlo sum spectrum, and the individual contributions from  $^{238}\text{U}$ ,  $^{232}\text{Th}$ ,  $^{40}\text{K}$ , and  $^{60}\text{Co}$ , as given by the best-fit, are shown. The derived activities and upper limits for this sample are given in Table 6.

## 5. Results

In this section, we first outline results obtained from a detailed study of the background of the facility, using the analysis method described in Section 4.2. We then present screening results for a few selected samples, the goal being to compare the outcome of the two analysis methods introduced in the previous section. Results from a much larger selection of screened samples are given and discussed in detail in [20].

### 5.1 Background Analysis

To model the residual background of the Gator facility, the detailed geometry of the crystal, cryostat system and shields has been simulated with Geant4. The following potential contributions to the background have been simulated: the natural decay chains of  $^{238}\text{U}$ ,  $^{232}\text{Th}$  and  $^{40}\text{K}$  decays in the copper of the shield and of the cryostat, the decays of the cosmogenic radio-nuclides  $^{54}\text{Mn}$ ,

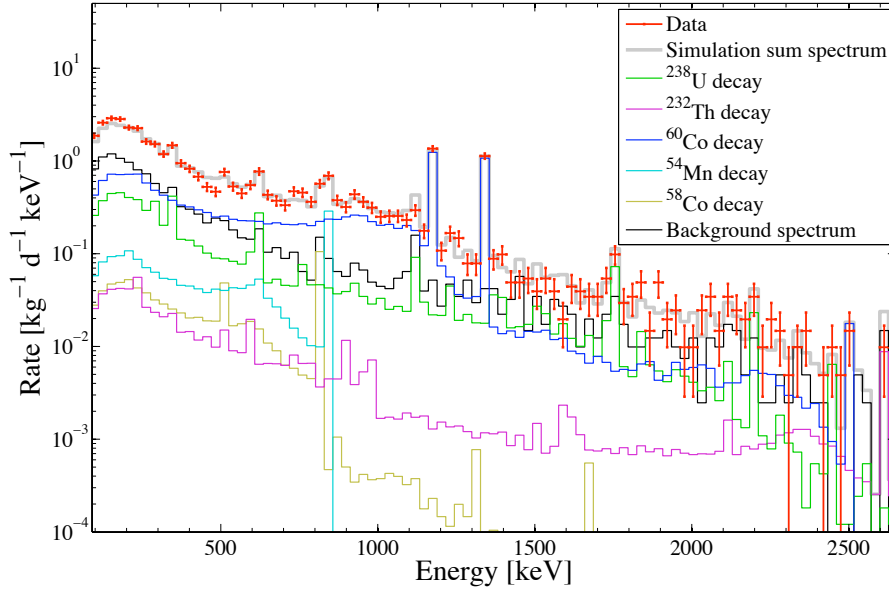


**Figure 5.** Best-fit of the Monte Carlo simulations to the measured data for a stainless steel sample. Data is shown with error bars (red), the full spectrum as determined by the simulation is shown as the grey solid curve. The individual contributions from the decays of  $^{60}\text{Co}$  (blue),  $^{238}\text{U}$  (green),  $^{232}\text{Th}$  (magenta),  $^{54}\text{Mn}$  (cyan) and  $^{58}\text{Co}$  (brown) are also shown, along with the measured background spectrum (black).

$^{65}\text{Zn}$ ,  $^{58}\text{Co}$ ,  $^{57}\text{Co}$ ,  $^{60}\text{Co}$  in the Ge crystal, the Cu of the cryostat and of the shield,  $^{210}\text{Pb}$  decays in the innermost Pb layer, and  $^{222}\text{Rn}$  decays inside the shield.<sup>2</sup> Other materials in the cryostat (PTFE, mylar and kapton) were neglected in the simulation due to their much lower mass compared to the copper (a few tens of grams and milligrams, respectively).

Figure 6 (top) shows the comparison of the latest measured Gator background to the sum spectrum obtained from the Monte Carlo simulations. On the bottom, the individual contributions of the main simulated background components are shown. The resulting activities for the individual chains and radio-nuclides, using the best fit of the data to the Monte Carlo simulations, are presented in Table 5. The background of the detector above  $\sim 500$  keV is thus currently dominated by the residual  $^{238}\text{U}$ ,  $^{232}\text{Th}$ ,  $^{40}\text{K}$  and  $^{60}\text{Co}$  activities in the Cu of the shield, and, to a lower extent, in the copper of the cryostat. Below  $\sim 500$  keV, the background is dominated by  $^{210}\text{Bi}$  bremsstrahlung from  $^{210}\text{Pb}$  decays in the innermost lead shield. The obtained  $^{210}\text{Pb}$  activity is with  $5.7 \pm 0.5$  Bq/kg higher than 3 Bq/kg, which is the value specified by the provider.

## 5.2 Sample Analysis

Prior to the screening of a specific sample, an estimate of the minimal measuring time  $t_{\min}$ , based on the mass, shape and the targeted activity  $A_{\text{target}}$  is performed:

$$t_{\min} = \frac{L_d}{A_{\text{target}} \cdot r \cdot m \cdot \epsilon}, \quad (5.1)$$

<sup>2</sup>A background run up to an energy of  $\sim 8$  MeV was acquired for a few weeks and revealed no U/Th contaminations close to the crystal, which would be visible as alpha peaks above a few MeV.

**Table 5.** Activities of residual and cosmogenic radionuclides inside the copper shield, the Ge crystal and the cryostat and of  $^{222}\text{Rn}$  inside the shield.

Isotope (chain)	Specific activity [ $\mu\text{Bq/kg}$ ]			Activity [ $\mu\text{Bq/m}^3$ ]	Activity [ $\text{Bq/kg}$ ]
	Cu (shield)	Ge crystal	Cu (cryostat)	Sample chamber	Inner Pb shield
$^{226}\text{Ra}$ ( $^{238}\text{U}$ )	$56 \pm 11$		$8 \pm 5$		
$^{228}\text{Th}$ ( $^{232}\text{Th}$ )	$27 \pm 7$		$4 \pm 2$		
$^{40}\text{K}$	$32 \pm 13$	$<1.30$	$11 \pm 6$		
$^{60}\text{Co}$	$8 \pm 4$	$<0.80$	$1.3 \pm 0.4$		
$^{58}\text{Co}$	$<0.27$	$<0.11$	$<0.22$		
$^{54}\text{Mn}$	$<1.30$	$<1.60$	$<2.15$		
$^{65}\text{Zn}$	$<0.16$	$<0.15$	$<0.50$		
$^{222}\text{Rn}$ ( $^{238}\text{U}$ )				$<55$	
$^{210}\text{Pb}$					$5.7 \pm 0.5$

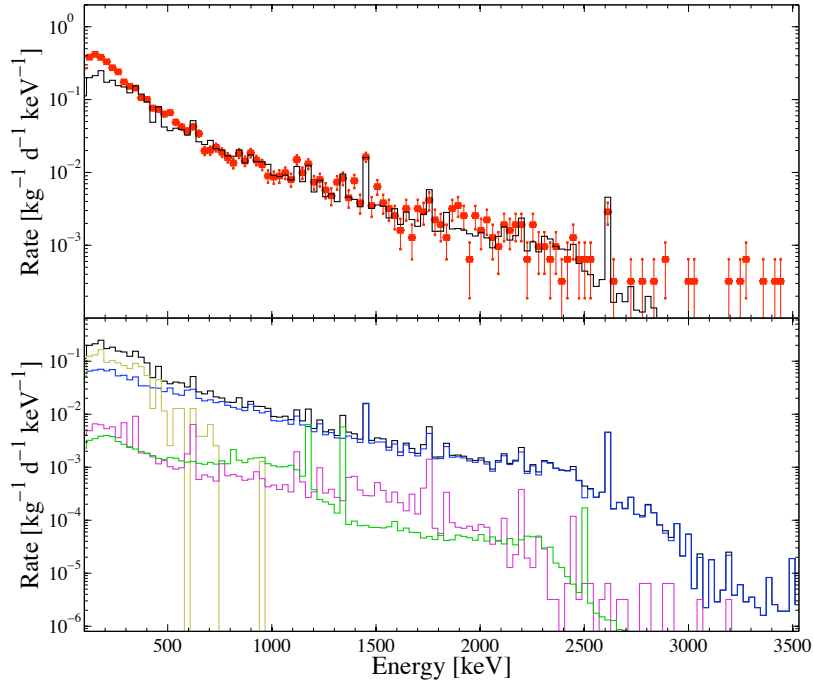


**Figure 6.** (Top) Comparison of the sum of the simulated spectra from natural and cosmogenic radionuclides in the detector and shield materials (black) with the observed background spectrum (red data points). (Bottom) The individual, best-fit contributions to the observed spectrum are shown: natural radioactivity in Cu (blue), cosmogenic radio-nuclides in Ge and Cu (green),  $^{222}\text{Rn}$  decays inside the shield (magenta) and  $^{210}\text{Pb}$  decays in the Pb shield (yellow).

where  $m$  is the mass of the sample,  $r$  is the branching ratio,  $\varepsilon$  is the detection efficiency and the detection limit  $L_d$  is defined in equation (4.2). Typical numbers for  $t_{\min}$  are 1-3 weeks in order to

achieve a sensitivity below a few mBq/kg. Figure 7 shows the sensitivity versus counting time for different sample masses using a specific gamma line (right) and for various radio-isotopes for a specific sample (left).

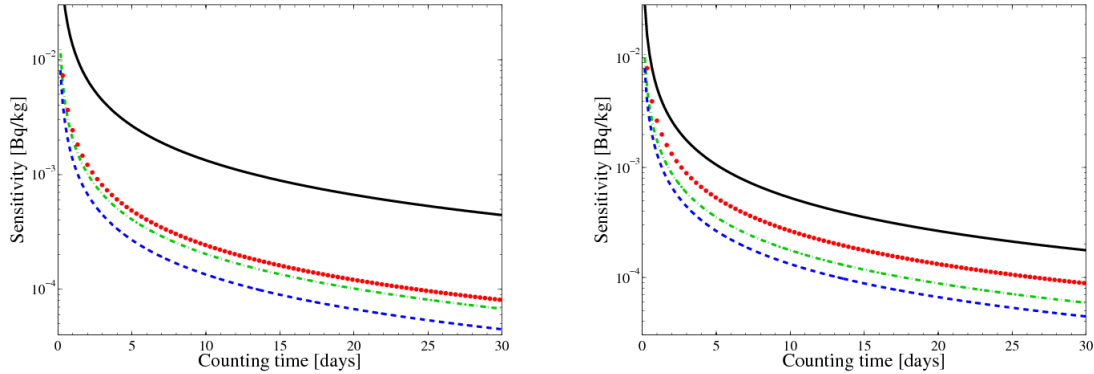


**Figure 7.** (Left) Sensitivity versus time for <sup>40</sup>K (black), the <sup>238</sup>U chain (using the <sup>214</sup>Bi 609 keV line, red), the <sup>232</sup>Th chain (using the <sup>212</sup>Pb 239 keV line, green) and <sup>60</sup>Co (blue) for a 13.5 kg sample of PTFE. (Right) Sensitivity versus counting time for different PTFE sample masses: 4 kg (black), 8 kg (red), 12 kg (green) and 16 kg (blue) using the 609 keV gamma line from <sup>214</sup>Bi.

The activities of the screened materials are calculated using the analysis methods described in Section 4.1 and 4.2. As evident from Table 6, where a few results from screened samples are provided, an excellent agreement between the results of the two methods was achieved. It provides a cross-check on the reliability of the used methods and on the obtained activities (or upper limits) for the samples that were screened. A large set of measurements is described and discussed in detail in [20].

**Table 6.** Comparison of results obtained by the two different analysis methods using four different screening samples.

Material (amount, time)	Method	Activity	<sup>226</sup> Ra	<sup>228</sup> Th	<sup>40</sup> K	<sup>60</sup> Co
Copper (18 kg, 20 d)	$\chi^2$	mBq/kg	<0.5	<0.5	<0.9	0.24 ± 0.08
	$\gamma$ -lines	mBq/kg	<0.3	<0.3	<1.3	0.24 ± 0.06
Stainless steel (6.6 kg, 6.8 d)	$\chi^2$	mBq/kg	4.1 ± 0.6	1.4 ± 0.4	<4.6	7.4 ± 1.1
	$\gamma$ -lines	mBq/kg	4.3 ± 0.9	<1.8	<5.7	7.2 ± 0.9
Concrete (35 g, 0.7 d)	$\chi^2$	Bq/kg	17 ± 2	3.1 ± 0.7	53 ± 4	<0.6
	$\gamma$ -lines	Bq/kg	15 ± 2	3.8 ± 0.8	42 ± 6	<0.7
Photomultipliers (22 pieces, 5.5 d)	$\chi^2$	mBq/PMT	<0.2	0.20 ± 0.09	8 ± 1	0.6 ± 0.1
	$\gamma$ -lines	mBq/PMT	<0.2	0.18 ± 0.06	11 ± 2	0.6 ± 0.1

## 6. Summary

The Gator screening facility at LNGS, described in detail in this paper, includes one of the world's

highest sensitivity HPGe spectrometers. It allows to measure large samples and to reach a sensitivity on specific activities below  $\sim$ mBq/kg when using typical sample masses of a few kg and measuring times extending from one to several weeks. The integral counting rate of the detector in the 100-2700 keV energy region has decreased by more than a factor of 5 from  $(0.842 \pm 0.005)$  counts/min at Soudan to  $(0.157 \pm 0.001)$  counts/min at LNGS. This decrease is mainly due to the improved shield and radon protection system, but also because of the decay of cosmogenic isotopes in the crystal and surrounding copper. The background of the facility, which was modeled using a detailed geometry of the spectrometer and its shield, and Monte Carlo simulations with Geant4, is dominated by U/Th/K decays in the copper of the cryostat and the shield, and from residual  $^{210}\text{Pb}$  in the innermost lead shield. This results from a comparison of background measurements with the simulations, by choosing the best fit of the MC spectra to the measured data. Two different data analysis methods show an excellent agreement when applied on a variety of samples. Detailed screening results for the XENON100 [5] experiment are presented and discussed in [20]. At present, the Gator facility is operated under stable conditions at LNGS. It is used to screen materials for the construction of the XENON1T experiment, for the next phase of the GERDA project, as well as for a future noble liquid dark matter search facility, DARWIN [19].

## 7. Acknowledgements

We thank James Beaty from the University of Minnesota for help with the detector operation at the Soudan laboratory and the machine shop crew at the RWTH Aachen, in particular Dipl. Ing. Michael Wlochal for the collaboration in the design and construction of the shield. We thank Giuseppina Mosca and Stefano Nisi from the chemistry lab at LNGS for the assistance in cleaning the samples, the LNGS staff, in particular Ing. Piergiorgio Aprili, for their continuous support and the XENON collaboration for the help in maintaining the facility. This work is supported by the Volkswagen Foundation, by the University of Zurich, and by the Swiss National Foundation Grant No. 20-118119 and No. 20-126993.

## References

- [1] G. Jungman, M. Kamionkowski, and K. Griest, Phys. Rept. **267**, 195 (1996), hep-ph/9506380.
- [2] G. Heusser, Ann. Rev. Nucl. Part. Sci. **45**, 543 (1995).
- [3] J. Angle et al. (XENON10 Collaboration), Phys. Rev. Lett. **100**, 021303 (2008), 0706.0039.
- [4] E. Aprile and L. Baudis, (XENON100 Collaboration), PoS **IDM2008**, 018 (2008), 0902.4253.
- [5] E. Aprile et al. (XENON100 Collaboration), Phys. Rev. Lett. **105**, 131302 (2010), 1005.0380.
- [6] E. Aprile et al. (XENON100 Collaboration) Phys. Rev. D **83**, 082001 (2011) 1101.3866.
- [7] Gerda experiment, <http://www.mpi-hd.mpg.de/gerda/home.html>.
- [8] M. L. H. Neder, G. Heusser, Applied Radiation and Isotopes **53**, 191 (2000).
- [9] G. Heusser, M. Laubenstein, N. Neder, Proc. of Intern. Conf. Isotop. Environm. (2004).
- [10] G. Knoll, *Radiation Detection and Measurement* (John Wiley and Sons, New York, 2000).
- [11] Canberra, <http://www.canberra.com/>.
- [12] Aurubis, <http://www.aurubis.com/en/home/>.
- [13] Plombum, <http://www.plombum.republika.pl/>.
- [14] SOLO facility, <http://particleastro.brown.edu/SOLO/>.
- [15] J. Angle, Ph.D. thesis, University of Florida, Florida (2008).
- [16] S. Agostinelli et al. (GEANT4), Nucl. Instrum. Meth. **A506**, 250 (2003).
- [17] M. Heisel, F. Kaether, and H. Simgen, Applied Radiation and Isotopes **67**, 741 (2009), ISSN 0969-8043.
- [18] C. Hurtgen, S. Jerome, and M. Woods, Applied Radiation and Isotopes **53**, 45 (2000), ISSN 0969-8043.
- [19] L. Baudis (DARWIN consortium) (2010), PoS **IDM2010**, 122 (2010), 1012.4764.
- [20] E. Aprile et al. (XENON100 Collaboration), Astroparticle Physics **35**, 43-49 (2011).